Accepted Manuscript

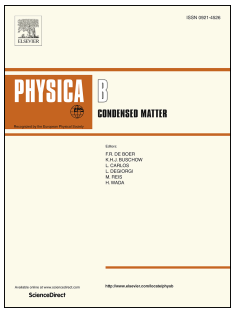

Post-deposition thermal treatment of sprayed ZnO:Al thin films for enhancing the conductivity

Sebin Devasia, P.V. Athma, Manu Shaji, M.C. Santhosh Kumar, E.I. Anila

PII: S0921-4526(18)30005-X

DOI: 10.1016/j.physb.2018.01.004

Reference: PHYSB 310651

To appear in: *Physica B: Physics of Condensed Matter*

Received Date: 11 November 2017

Revised Date: 1 January 2018

Accepted Date: 2 January 2018

Please cite this article as: S. Devasia, P.V. Athma, M. Shaji, M.C.S. Kumar, E.I. Anila, Post-deposition thermal treatment of sprayed ZnO:Al thin films for enhancing the conductivity, *Physica B: Physics of Condensed Matter* (2018), doi: 10.1016/j.physb.2018.01.004.

Post-deposition thermal treatment of sprayed ZnO:Al thin films for enhancing the conductivity

Sebin Devasia[a], P V Athma[a,b], Manu Shaji[c], M C Santhosh Kumar[d], E I Anila[a,*]

[a] *Optoeletronic and Nanomaterials Research Laboratory, Department of Physics, Union Christian College, Aluva, Kerala 683102 India*
[b] *Department of Physics, SNM College, Maliankara 683 516, India*
[c] *Nanophotonic and Optoelectronic Devices Laboratory, Department of Physics, Cochin University of Science and Technology, Kochi 682 022 India*
[d] *Optoelectronic Materials and Devices Lab, Department of Physics, National Institute of Technology, Tiruchirappalli 620015, India*

Abstract

Here, we report the enhanced conductivity of Aluminium doped ($2at.\%$) zinc oxide thin films prepared by simple spray pyrolysis technique. The structural, optical, electrical, morphological and compositional investigations confirm the better quality of films that can be a potential candidate for application in transparent electronics. Most importantly, the film demonstrates an average transmittance of 90 percent with a low resistivity value which was dropped from 1.39×10^{-2} to $5.10 \times 10^{-3}\Omega.cm$, after annealing, and a very high carrier concentration in the order of $10 \times 20cm^{-3}$. Further, we have used the Swanepoel envelop method to calculate thickness, refractive index and extinction coefficient from the interference patterns observed in the transmission spectra. The calculated figure of merit of the as-deposited sample was $1.4 \times 10^{-3}\Omega^{-1}$ which was improved to $2.5 \times 10^{-3}\Omega^{-1}$ after annealing.

Keywords: Spray pyrolysis, ZnO, Al doping, TCO, Refractive index, Swanepoel method

*Corresponding author
Email address: anilaei@gmail.com (E I Anila)

1. Introduction

Design for a variety of optoelectronic devices demand materials with an ideal combination of high electrical conductivity and optical transparency which are hard to achieve in the same material. However, doped wide band gap semiconductors of low carrier effective mass have the potential to overcome this hurdle. A majority of transparent conductors realised up to date are based on post-transition metal cations, such as In^{3+}[1], Sn^{4+}[2], Cd^{2+}[3] and Zn^{2+}[4], which have widespread s-orbitals. The indium and tin based TCOs were used extensively because of their better electronic and optical properties. But the scarcity of Indium and hike in price of tin had led to the search for alternate materials. ZnO has been recognised as a suitable substitute because of its low cost, greater abundance and comparable properties with counterparts[5].

Research over the past decade has proved that ZnO thin films can be efficiently used as a transparent conducting oxide in a variety of devices like LEDs[6], laser diodes[7], photodetectors[8], vacuum fluorescent and field emission displays[9], sensors and integrated non-linear optical devices[10]. ZnO has a direct and wide band gap of 3.37 eV with a very high transmittance in the visible spectral region. Moreover, its large single crystals can be grown in the hexagonal wurtzite structure. A wide range of applications has been suggested based on its properties like large free exciton binding energy (60 meV), large piezoelectric constants, strong luminescence as well as strong sensitivity to various adsorbed species, large non-linear optical coefficients, high thermal conductivity, radiation hardness and amenability to wet chemical etching [11, 4, 12].

ZnO is intrinsically n-type which is proposed to be due to shallow donors like oxygen vacancies and zinc interstitials[13]. This n-type conductivity in ZnO can be enhanced by doping with shallow donor impurities like B [14], Al, Ga[15], In[16], F[17] and H[18]. Particularly, doping ZnO with aluminium have been tremendously studied because of its high conductivity comparable to its counterpart, ITO. It has low formation energy and an ionization energy of 120 meV. Aluminium (Al^{3+}), a group-III element, is incorporated into the crystal

lattice by substituting Zn^{2+} ions (Zn^{2+}:0.74 $\AA$; Al^{3+}:0.54 $\AA$). This generates loosely bound additional valence electron that occupies states near conduction band minimum (CBM) and can be excited to conduction band on the supply of sufficient energy[19].

A number of thin film deposition techniques have been used by researchers for deposition of TCOs, which includes pulsed laser deposition[6], thermal evaporation[20], chemical vapour deposition[21], sol-gel[22], RF magnetron sputtering[23] and spray pyrolysis[24, 25, 26]. Among these techniques, spray pyrolysis is an effective method for large area deposition of thin films without any high vacuum atmospheres. Thus making it a suitable method to substantially reduce the time and cost of production. In addition to that, the morphology and thickness of the films can be controlled by tuning various deposition parameters like spray rate, substrate to nozzle distance, substrate temperature, atomizing pressure etc.[24].

Even though in 1991, Aktaruzzaman had achieved a resistivity of 4.7×10^{-3} Ωcm, they used N2 as the carrier gas during spray deposition[25]. Later, Achour et al achieved the lowest resistivity of 3×10^{-3} Ωcm was again using N2 as carrier gas[26]. Here, we have fabricated ZnO:Al thin films with compressed air as the carrier gas and achieved similar conductivity value with an average transmittance of 90% in the visible spectrum (400 - 700 nm). This suggests the potential of spray pyrolysis technique to fabricate high-quality ZnO:Al thin films that can be used as a transparent electrode in various optoelectronic devices[27].

2. Materials and Methods

A 0.2 M precursor solution was prepared from high purity zinc acetate ($Zn(CH_3COO)_2.2H_2O$, MERK, 98%) and aluminium acetylacetonate ($C_{15}H_{21}AlO_6$, Sigma-Aldrich, 99%) in a solvent mixture of propanol and water (7:3). A small amount (3 ml) of acetic acid was added to suppress the precipitation of zinc hydroxide and to stabilize the solution.

Soda lime glass slides ($75 \times 25 \times 1$ mm) were used as substrates to deposit

thin films. After cleaning with soap solution and distilled water glass slides were kept in chromic acid for 2 hours, which were then sonicated for 30 minutes in distilled water. Then they were cleaned with distilled water, acetone, propanol and distilled water respectively.

An automated spray pyrolysis system (HO-TH-04: Holmarc) was used for the deposition of films onto glass slides. The optimized spray parameters like spray rate, deposition time and area of deposition were controlled by a spray pyrolysis software. The substrate to spray head nozzle distance was kept as 10 cm and the substrate temperature was 425 ^0C. The solution was loaded into the glass containers attached to a microprocessor based dispensing system which uses a stepper motor controlled piston to dispense the solution. The coating solution was atomized and sprayed onto the substrate with the help of pressurised air from a compressor. The substrates were heated to 425 ^0C by a substrate heater controlled by PID temperature controller.

The as-deposited films were annealed at 450^0C for one hour in the vacuum ($\sim 2 \times 10^{-5}$ bar). We have then characterized the samples for understanding its various properties. The crystalline phases of the samples were identified using X-ray diffraction technique using a Bruker AXS D8 Advance diffractometer ($CuK_\alpha - 1.5406$ Å). Hall effect measurements were taken using ECOPIA:HMS-5000 system in van der paw technique to investigate the electronic properties. Activation energies were calculated from the temperature-dependent conductivity measurements. UV-Vis-NIR spectroscopy (JASCO V670) was used to obtain the transmittance and optical band gap. Photoluminescence measurements were taken using a Fluoromax-4 spectrofluorometer. The morphology of the films were analysed using atomic force microscopy (AFM) and scanning electron microscopy (SEM). The composition of the samples were investigated using energy dispersive X-ray (EDX) spectrum.

3. Results and Discussion

3.1. Structural Analysis

X-ray diffraction measurements were carried out to investigate the various crystalline phases present in the sample. Figure 1(a) reveals the preferentially c-axis oriented hexagonal wurtzite phase of the samples. The Bragg reflections corresponding to (100), (002), (101), (102) and (103) of ZnO (JCPDS Card No: 89-0510) were observed. No other crystalline phases corresponding to Al_2O_3 or Zn-Al-O complexes were found. This confirms the successful growth of single phase ZO:Al films on the glass substrates.

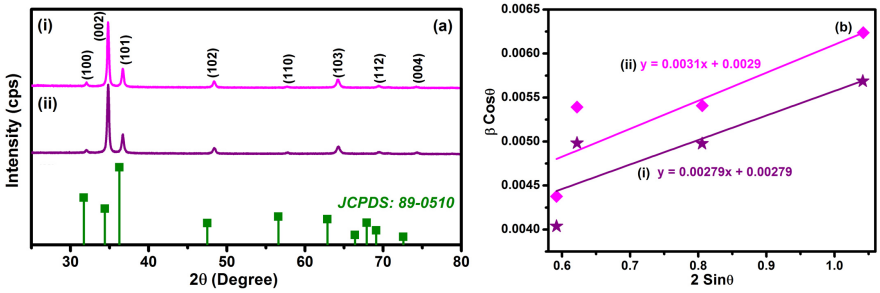

Figure 1: (a) XRD profiles of the (i) as-deposited and (ii) annealed samples of ZnO:Al ($2at.\%$) thin films. (b) The Williamson Hall plots drawn to determine the strain in films.

However, only negligible changes were observed in the structural properties of the sample after annealing. The crystallite size (D) was perceived to be increasing from 26 nm to 29 nm, which was computed from the Scherrer formula[28],

$$D = (0.9\lambda)/(\beta \cos\theta) \tag{1}$$

Where, λ is the wavelength of CuK_α radiation (1.5406 Å), β is the FWHM and θ is the Bragg diffraction angle. It was suggested that as a result of vacuum annealing the smaller $Al^{3+}(r_{Al^{3+}} = 0.54$ Å) ions were secluded from the substitutional $Zn^{2+}(r_{Zn^{2+}} = 0.74$ Å) sites to grain boundaries leading to a reduced localized lattice distortion which might have slightly improved the

crystallinity[29]. The microstrain present in the crystal lattice, along the c-axis, was calculated from the Williamson-Hall plots, illustrated in Figure 2(b), employing the equation[30],

$$\beta_{hkl} \cos\theta = \frac{k\lambda}{D} + 4\epsilon \sin\theta \tag{2}$$

The stress (G) can be calculated from[31],

$$G = -453.6 \times 10^9 \times \epsilon \tag{3}$$

Where, ϵ is the strain value observed from the W-H plot. The as-deposited films show a tensile stress of 0.325 GPa which was slightly increased to 0.371 GPa after annealing.

3.2. Electrical Studies

Table 1 presents the electrical properties of samples obtained from the Hall effect measurements at room temperature in van der paw configuration. The conductivity of the samples was found to be improved on annealing. The observed resistivity value of the as-deposited sample was 1.39×10^{-2} Ωcm which on annealing reduced to 5.10×10^{-3} Ωcm. The Carrier concentration of the samples was substantially high in the order of 10^{20} cm^{-3} with a mobility that rose slightly from 3.45 $cm^2V^{-1}s^{-1}$ to 3.74 $cm^2V^{-1}s^{-1}$ on annealing.

Table 1: Electrical parameters of the as deposited and annealed ZO:Al samples from Hall effect Measurements.

Sample	**Resistivity** (Ωcm)	**Carrier concentration** (cm^{-3})	**Mobility** ($cm^2V^{-1}s^{-1}$)
As deposited	1.39×10^{-2}	1.30×10^{20}	3.45
Annealed	5.10×10^{-3}	3.27×10^{20}	3.74

The low resistivity value of the as-deposited sample is due to the efficient substitution of Zn^{2+} ions by the Al^{3+} ions, which supplies one extra free electron/atom in the crystal lattice. The resistivity value was further reduced on annealing which is attributed to the increased mobility and carrier concentration in the sample. These enhanced electrical properties may be as a result of the increase in oxygen vacancies and desorption of oxygen from grain boundaries during thermal treatment in vacuum[32, 33, 34].

Furthermore, we have studied the electronic properties in detail by observing the variation of resistivity values with temperature in the range of 315 K to 420 K. Resistivity was found to decrease with temperature as more charge carriers were generated by thermal excitation and desorption of oxygen which suggests semiconducting behaviour[35].

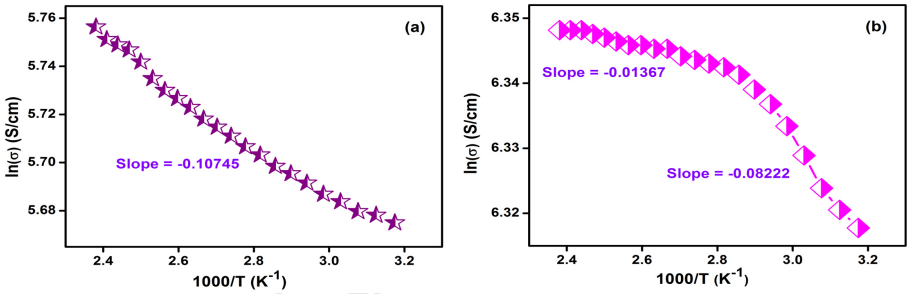

Figure 2: The Arrhenius plots of (a) as deposited and (b) annealed samples drawn between ln(σ) and 1/T for the determination of activation energy.

We know that in n-type semiconductors, a minimum energy corresponding to E_C-E_D is needed to ionize the donor levels for activation of electrical conductivity. Here, E_C is the conduction band minimum and E_D is the donor level maximum. In the case of ZnO, which have deeper donor levels, the electrical conductivity depends significantly on carrier concentration (n) which increases on thermal excitation. Figure 2(a) and 2(b) shows the Arrhenius plot drawn to calculate the thermal activation energy for electrical conduction using the equation[36],

$$\sigma = \sigma_0 exp(-E_a/kT) \quad (4)$$

Where σ is the electrical conductivity, σ_0 is a constant depending on the nature of thin films and E_a is the activation energy.

Calculated activation energy of the as-deposited film was 9.26 meV which after annealing in vacuum reduced to 1.17 meV in the region 420 - 355 K and 7.08 meV in the region 355 315 K. The enhanced donor concentration shifts the Fermi level up in the band gap which results in the decrease of activation energy after annealing of ZO:Al samples[35].

3.3. Photoluminescence Spectroscopy

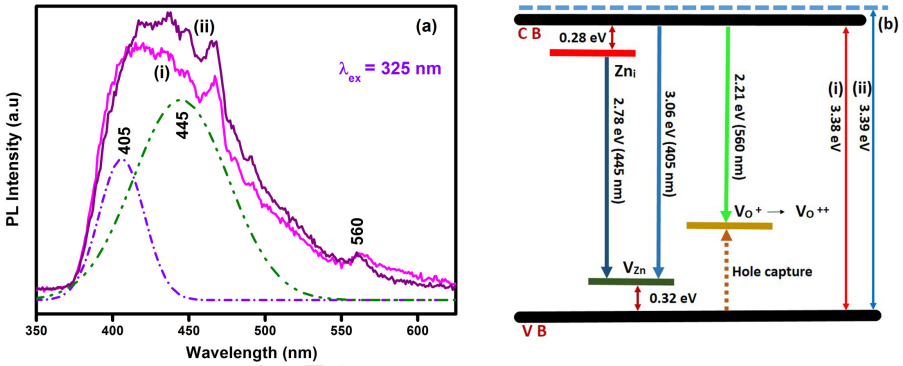

Figure 3: (a) Photoluminescence spectra of the (i) as-deposited and (ii) annealed ZnO:Al films. (b) The band energy diagram reveals the calculated defect levels from PL.

Photoluminescence is an efficient characterization tool to analyse the defects present in the sample. The PL spectra of the as-deposited and annealed samples excited at a wavelength of 325 nm are given in figure 3(a). The violet emission at 405 nm (3.06 eV) may be the $CB \rightarrow V_{Zn}$ transition as suggested by Jeong et al.[37] Considering the blue region of PL spectra, the peak at 445 nm (2.78 eV) corresponds to the transition $Zn_i \rightarrow V_{Zn}$[38, 39]. The less intense green region is generally attributed to the oxygen-related defects. Vanheusden et al. suggests the formation of doubly ionized oxygen vacancies ($V_{O^{++}}$) which

radiatively recombines with a photoexcited hole as a possible origin of peak at 560 nm (2.21 eV)[40].

3.4. UV-Vis-NIR Spectroscopy

Figure 4 indicates the transmission spectra of the as-deposited and annealed ZnO:Al films in the wavelength range of 310 - 1500 nm. The band edge absorption causes a sharp plummet at 360 nm. The as-deposited sample showed an average transmittance above 90% which have displayed a slight reduction after annealing. This reduced transmission value in annealed films is due to the increased phonon scattering and free carrier absorption of photons as annealing results in higher concentration of free charge carriers and increased mobility. The observed interference fringes suggests that the films are smooth on the surface and on the interface with glass substrate[41].

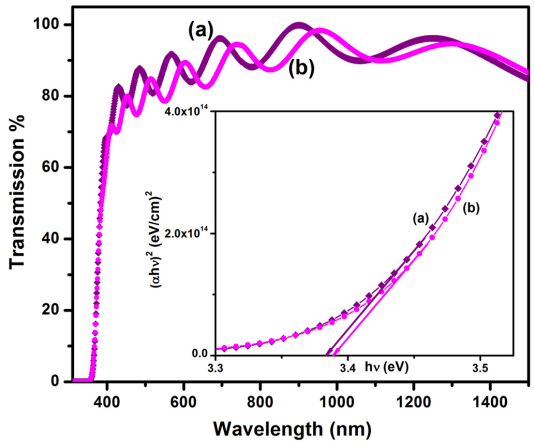

Figure 4: The transmittance curves of (a) as-deposited and (b) annealed ZnO:Al films. The inset depicts the taucs plots drawn for (a) as-deposited and (b) annealed films to find the bandgap values.

Semiconductors absorb photons corresponding to the band gap energy. The absorption coefficient (α) can be calculated from Lamberts formula[42],

$$\alpha = \frac{1}{t} log(1/T) \tag{5}$$

Where, t and T are the thickness and the transmittance value, respectively. The band gap energy (E_g) of the samples can be calculated from the taucs relation[43],

$$(\alpha h\nu)^2 = h\nu - E_g \tag{6}$$

A typical $(\alpha h\nu)^2$ vs. $h\nu$ graph is shown in the inset of figure 4. The observed value for band gap of the as-deposited sample is 3.38 eV which was blue shifted to 3.39 eV for annealed sample. This increase in optical band gap arises due to the Burstein-Moss (BM) band filling effect which is defined as the widening of the band gap due to the increased carrier concentration. As a result of the large number of charge carriers in the film, the density of states near the conduction band minimum will be occupied and optical transitions are allowed only to a higher energy state satisfying the Fermi exclusion principle[44, 45].

The quality of the transparent conducting oxide films is determined by figure of merit (ϕ), which can be calculated from the resistivity and transmittance data using the following equation proposed by Haacke[46],

$$\phi = T^{10}/R_s \tag{7}$$

Where R_s is the sheet resistance and T is the transmittance. The calculated figure of merit value for the as-deposited sample and annealed samples were $1.4 \times 10^{-3-1}$ and $2.5 \times 10^{-3-1}$, respectively.

We have then used an envelope method, originally proposed by Manifacier et al.[47] and later reported by Swanepoel[48], to obtain the thickness of the film from the interference patterns in the transmission curve. Figure 5 represents the envelopes $T_{max}(\lambda)$ and $T_{min}(\lambda)$ fitted using the origin software. The thickness (t) of the films can be calculated from the following equation,

$$t = \frac{\lambda_1 \lambda_2}{2[n(\lambda_1)\lambda_2 - n(\lambda_2)\lambda_1]} \tag{8}$$

Where, $\lambda_1$and λ_2 are the consecutive maxima or minima. $n(\lambda_1)$ and $n(\lambda_2)$ are the refractive indices of the samples at λ_1 and λ_2. The refractive index of the film as a function of wavelength can be found from the equations,

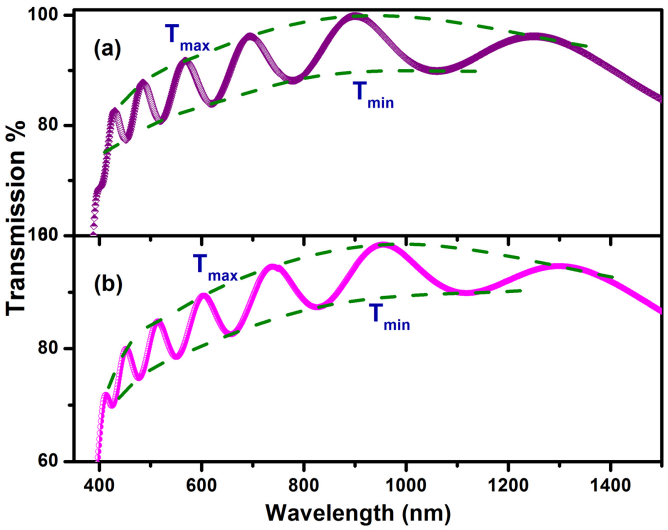

Figure 5: The envelopes drawn on the UV-Vis-NIR transmission curves of the (a) as deposited and (b) annealed ZnO:Al films using Origin software.

$$n = [N + (N^2 - n_0 n_s)^2]^{1/2} \tag{9}$$

Where,

$$N = \frac{(n_0^2 + n_s^2)}{2} + 2n_0 n_s \times \frac{(T_{max} - T_{min})}{T_{max} T_{min}} \tag{10}$$

Here, n_0 is the refractive index of air (= 1) and n_s is the refractive index of substrate (= 1.52). T_{max} and T_{min} are the values in the upper and lower envelope at the same wavelength.

The calculated refractive indices of the films as a function of wavelength in the visible spectrum is illustrated in figure 6(a). After a gradual increase from 1.75 at 400 nm to 1.84 at 495 nm, the refractive index of the as-deposited film is observed to be around 1.83. The annealed films shows slightly low refractive index than as-deposited films at 400 nm, amounting to a value of 1.64. Then it follows a steep increase to 1.85 at 455 nm and then fluctuates around 1.82 in the visible spectrum. The slightly reduced value of refractive index may be due to an increased carrier concentration after vacuum annealing[49].

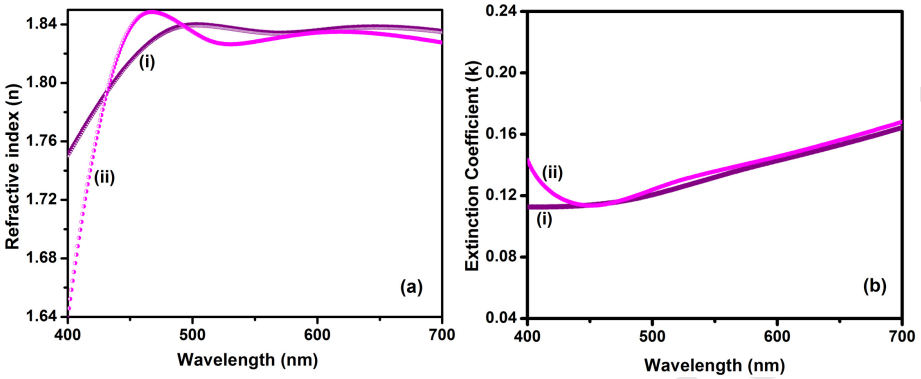

Figure 6: The (a) refractive index $n(\lambda)$ and (b) extinction coefficient $k(\lambda)$ of (i) as-deposited and (ii) annealed ZnO:Al thin films calculated by Swanepoel method.

Since, the refractive index as a function of wavelength was calculated, the thickness can be calculated from equation 8. The calculated thickness of the films are 0.84 and 0.85 m for the as-deposited and annealed films, respectively.

The extinction coefficient (k) was also calculated from the data obtained through envelope method. It was calculated using the equation[48],

$$k = \frac{\alpha\lambda}{4\pi} \tag{11}$$

Where , the absorption coefficient, can be calculated from,

$$\alpha = \frac{1}{t} ln \frac{(n-n_0)(n-n_s)[(T_{max}/T_{min})^{1/2}+1])}{(n+n_0)(n-n_s)[(T_{max}/T_{min})^{1/2}-11]} \tag{12}$$

The extinction coefficient as a function of wavelength is shown in the figure 6(b). The extinction coefficient follows a gradual linear increase with wavelength, 0.11 (450 nm) to 0.16 (700 nm), in the visible spectrum.

3.5. Atomic Force Microscopy

To analyse the variation in surface topography due to annealing, AFM studies were carried out for the samples. Figure 7 shows the AFM images of the samples from which the root mean square surface roughness (RMSSR) was calculated by using the WSxM software[50].

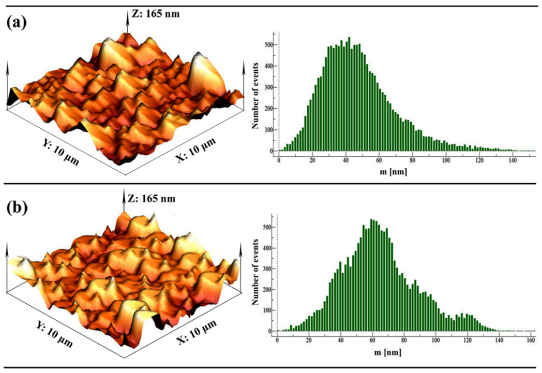

Figure 7: AFM micro-graphs of the (a) as-deposited and (b) annealed samples. The root mean square surface roughness measurements of the samples are shown on the right side.

The as-deposited and annealed films showed a surface roughness of 21.6 nm and 23.5 nm, respectively. The observed values show a slight increase in surface roughness as a result of annealing. The high values of surface roughness may be due to the large particle sizes formed from the coalesced grains.

3.6. Scanning Electron Microscopy

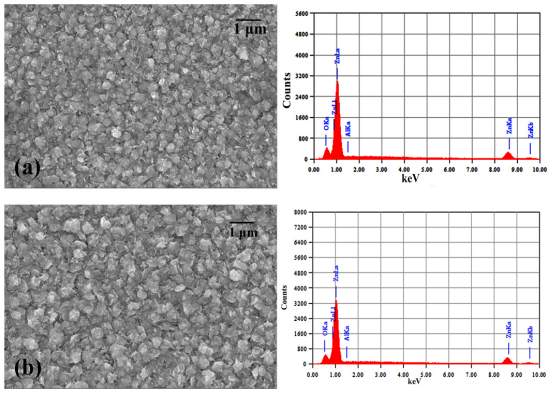

Figure 8: The SEM images of the (a) as-deposited and (b) annealed ZO:Al samples along with the EDX spectrum.

The surface morphology of the samples was analysed using Scanning Electron Microscopy (SEM) using a JEOL JSM-6490 instrument and is illustrated in

figure 8.

The SEM images of as-deposited and annealed films reveal that the particles are uniformly distributed over the surface. The particles in the as-deposited samples have agglomerated to form larger grains. Compositional analysis by Energy Dispersive X-ray measurements shows the presence of zinc, oxygen and aluminium in the samples. The Al/Zn atomic concentration was 1.6% and 2.2% for the as-deposited and annealed samples, respectively. This proves the successful incorporation of aluminium which improved the conductivity of the samples.

4. Conclusions

We have deposited 2 at%. aluminium doped zinc oxide thin films onto glass substrates which were then annealed at 450 ^0C. Different properties of the pre and post-annealed samples were investigated. The structural, optical and morphological studies done by x-ray diffraction, photoluminescence and UV-Vis-NIR spectroscopy, atomic force microscopy and scanning electron microscopy suggests the deposition of good quality films. The post annealing of the samples in vacuum have significantly enhanced the shallow donor levels in the sample which has resulted in the enhanced conductivity. We have observed a high conductivity of 5.10×10^{-3} Ωcm with a carrier concentration of 3.27×10^{20} cm^{-3} for the films after annealing in vacuum. The films showed an average transmission of 90 percentage in the visible range. The thickness calculated using envelope method was 835 nm and 850 nm for as-deposited and annealed films, respectively. The calculated figure of merit values suggest that the films deposited are of good quality which can be used as transparent electrodes in device fabrication.

5. Acknowledgement

This work was supported by Department of Atomic Energy (DAE), Board of Research in Nuclear Sciences (BRNS) (sanction no: 34/14/58/2014-BRNS).

The authors are grateful to Centre for Advanced Materials, Cochin University of Science and Technology, India for providing characterization facilities.

References

[1] R. B. H. Tahar, T. Ban, Y. Ohya, Y. Takahashi, Electronic transport in tin-doped indium oxide thin films prepared by sol-gel technique, Journal of applied physics 83 (4) (1998) 2139–2141.

[2] E. Comini, G. Faglia, G. Sberveglieri, Uv light activation of tin oxide thin films for no2 sensing at low temperatures, Sensors and Actuators B: Chemical 78 (1-3) (2001) 73–77.

[3] A. J. Varkey, A. Fort, Transparent conducting cadmium oxide thin films prepared by a solution growth technique, Thin Solid Films 239 (2) (1994) 211–213.

[4] A. Mang, K. Reimann, et al., Band gaps, crystal-field splitting, spin-orbit coupling, and exciton binding energies in zno under hydrostatic pressure, Solid state communications 94 (4) (1995) 251–254.

[5] A. Janotti, C. G. Van de Walle, Fundamentals of zinc oxide as a semiconductor, Reports on progress in physics 72 (12) (2009) 126501.

[6] H. Kim, C. Gilmore, J. Horwitz, A. Pique, H. Murata, G. Kushto, R. Schlaf, Z. Kafafi, D. Chrisey, Transparent conducting aluminum-doped zinc oxide thin films for organic light-emitting devices, Applied Physics Letters 76 (3) (2000) 259–261.

[7] H. Liang, S. Yu, H. Yang, Directional and controllable edge-emitting zno ultraviolet random laser diodes, Applied Physics Letters 96 (10) (2010) 101116.

[8] Y. Liu, C. Gorla, S. Liang, N. Emanetoglu, Y. Lu, H. Shen, M. Wraback, Ultraviolet detectors based on epitaxial zno films grown by mocvd, Journal of Electronic Materials 29 (1) (2000) 69–74.

[9] Y. Nakanishi, A. Miyake, H. Kominami, T. Aoki, Y. Hatanaka, G. Shimaoka, Preparation of zno thin films for high-resolution field emission display by electron beam evaporation, Applied Surface Science 142 (1) (1999) 233–236.

[10] M. Larciprete, D. Haertle, A. Belardini, M. Bertolotti, F. Sarto, P. Günter, Characterization of second and third order optical nonlinearities of zno sputtered films, Applied Physics B: Lasers and Optics 82 (3) (2006) 431–437.

[11] D. Thomas, The exciton spectrum of zinc oxide, Journal of Physics and Chemistry of Solids 15 (1-2) (1960) 86–96.

[12] V. Coleman, C. Jagadish, Zinc oxide bulk, thin films and nanostructures, UK, Elsevier (2006) 1–5.

[13] S. E. Harrison, Conductivity and hall effect of zno at low temperatures, Physical Review 93 (1) (1954) 52.

[14] X. Chen, B. Xu, J. Xue, Y. Zhao, C. Wei, J. Sun, Y. Wang, X. Zhang, X. Geng, Boron-doped zinc oxide thin films for large-area solar cells grown by metal organic chemical vapor deposition, Thin Solid Films 515 (7) (2007) 3753–3759.

[15] H. Gomez, A. Maldonado, M. d. l. L. Olvera, D. Acosta, Gallium-doped zno thin films deposited by chemical spray, Solar energy materials and solar cells 87 (1) (2005) 107–116.

[16] P. R. Kumar, C. S. Kartha, K. Vijayakumar, T. Abe, Y. Kashiwaba, F. Singh, D. Avasthi, On the properties of indium doped zno thin films, Semiconductor Science and Technology 20 (2) (2005) 120–126.

[17] H. Yoon, K. Lee, T. Lee, B. Cheong, D. Choi, D. Kim, W. Kim, Properties of fluorine doped zno thin films deposited by magnetron sputtering, Solar Energy Materials and Solar Cells 92 (11) (2008) 1366–1372.

[18] L.-Y. Chen, W.-H. Chen, J.-J. Wang, F. C.-N. Hong, Y.-K. Su, Hydrogen-doped high conductivity zno films deposited by radio-frequency magnetron sputtering, Applied physics letters 85 (23) (2004) 5628–5630.

[19] S. Zhang, S.-H. Wei, A. Zunger, Intrinsic n-type versus p-type doping asymmetry and the defect physics of zno, Physical Review B 63 (7) (2001) 075205.

[20] S. N. F. Hasim, M. A. A. Hamid, R. Shamsudin, A. Jalar, Synthesis and characterization of zno thin films by thermal evaporation, Journal of Physics and Chemistry of Solids 70 (12) (2009) 1501–1504.

[21] S. Chen, R. M. Wilson, R. Binions, Synthesis of highly surface-textured zno thin films by aerosol assisted chemical vapour deposition, Journal of Materials Chemistry A 3 (11) (2015) 5794–5797.

[22] L. Znaidi, G. S. Illia, S. Benyahia, C. Sanchez, A. Kanaev, Oriented zno thin films synthesis by sol–gel process for laser application, Thin Solid Films 428 (1) (2003) 257–262.

[23] T. T. T. Vo, Y.-H. Ho, P.-H. Lin, Y. Tai, Control of growth mode and crystallinity of aluminium-doped zinc oxide thin film at room temperature by self-assembled monolayer assisted modulation on substrate surface energy, CrystEngComm 15 (34) (2013) 6695–6701.

[24] P. S. Patil, Versatility of chemical spray pyrolysis technique, Materials Chemistry and physics 59 (3) (1999) 185–198.

[25] A. Aktaruzzaman, G. Sharma, L. Malhotra, Electrical, optical and annealing characteristics of zno: Al films prepared by spray pyrolysis, Thin solid films 198 (1-2) (1991) 67–74.

[26] Z. B. Achour, T. Ktari, B. Ouertani, O. Touayar, B. Bessais, J. B. Brahim, Effect of doping level and spray time on zinc oxide thin films produced by spray pyrolysis for transparent electrodes applications, Sensors and Actuators A: Physical 134 (2) (2007) 447–451.

[27] K. Ravichandran, N. Jabena Begum, S. Snega, B. Sakthivel, Properties of sprayed aluminum-doped zinc oxide filmsa review, Materials and Manufacturing Processes 31 (11) (2016) 1411–1423.

[28] Y.-S. Kim, W.-P. Tai, Electrical and optical properties of al-doped zno thin films by sol–gel process, Applied Surface Science 253 (11) (2007) 4911–4916.

[29] S. D. Shinde, S. Date, A. V. Deshmukh, A. Das, P. Misra, L. Kukreja, K. Adhi, Role of al doping in structural, microstructural, electrical and optical characteristics of as-deposited and annealed zno thin films, RSC Advances 5 (31) (2015) 24178–24187.

[30] A. K. Zak, W. A. Majid, M. E. Abrishami, R. Yousefi, X-ray analysis of zno nanoparticles by williamson–hall and size–strain plot methods, Solid State Sciences 13 (1) (2011) 251–256.

[31] Z. Fang, Z. Yan, Y. Tan, X. Liu, Y. Wang, Influence of post-annealing treatment on the structure properties of zno films, Applied Surface Science 241 (3) (2005) 303–308.

[32] H.-m. Zhou, D.-q. Yi, Z.-m. Yu, L.-r. Xiao, J. Li, Preparation of aluminum doped zinc oxide films and the study of their microstructure, electrical and optical properties, Thin solid films 515 (17) (2007) 6909–6914.

[33] F. Ruske, M. Roczen, K. Lee, M. Wimmer, S. Gall, J. Hüpkes, D. Hrunski, B. Rech, Improved electrical transport in al-doped zinc oxide by thermal treatment, Journal of Applied Physics 107 (1) (2010) 013708.

[34] W. Cranton, N. Kalfagiannis, X. Hou, R. Ranson, D. Koutsogeorgis, et al., Enhanced electrical and optical properties of room temperature deposited aluminium doped zinc oxide (azo) thin films by excimer laser annealing, Optics and Lasers in Engineering 80 (2016) 45–51.

[35] R. Kumar, N. Khare, Temperature dependence of conduction mechanism of zno and co-doped zno thin films, Thin Solid Films 516 (6) (2008) 1302–1307.

[36] G. Rusu, M. Popa, G. Rusu, I. Salaoru, On the electronic transport properties of polycrystalline znse films, Applied surface science 218 (1) (2003) 223–231.

[37] S.-H. Jeong, B.-S. Kim, B.-T. Lee, Photoluminescence dependence of zno films grown on si (100) by radio-frequency magnetron sputtering on the growth ambient, Applied Physics Letters 82 (16) (2003) 2625–2627.

[38] E. Bylander, Surface effects on the low-energy cathodoluminescence of zinc oxide, Journal of Applied Physics 49 (3) (1978) 1188–1195.

[39] B. Lin, Z. Fu, Y. Jia, Green luminescent center in undoped zinc oxide films deposited on silicon substrates, Applied Physics Letters 79 (7) (2001) 943–945.

[40] K. Vanheusden, W. Warren, C. Seager, D. Tallant, J. Voigt, B. Gnade, Mechanisms behind green photoluminescence in zno phosphor powders, Journal of Applied Physics 79 (10) (1996) 7983–7990.

[41] S. T. Tan, B. Chen, X. Sun, W. Fan, H. S. Kwok, X. Zhang, S. Chua, Blueshift of optical band gap in zno thin films grown by metal-organic chemical-vapor deposition, Journal of Applied Physics 98 (1) (2005) 013505.

[42] R. Ghosh, G. Paul, D. Basak, Effect of thermal annealing treatment on structural, electrical and optical properties of transparent sol–gel zno thin films, Materials research bulletin 40 (11) (2005) 1905–1914.

[43] O. Lupan, T. Pauporté, L. Chow, B. Viana, F. Pellé, L. Ono, B. R. Cuenya, H. Heinrich, Effects of annealing on properties of zno thin films prepared by electrochemical deposition in chloride medium, Applied Surface Science 256 (6) (2010) 1895–1907.

[44] J. Lu, S. Fujita, T. Kawaharamura, H. Nishinaka, Y. Kamada, T. Ohshima, Z. Ye, Y. Zeng, Y. Zhang, L. Zhu, et al., Carrier concentration dependence of band gap shift in n-type zno: Al films, Journal of Applied Physics 101 (8) (2007) 083705.

[45] D. Garcia-Alonso, S. E. Potts, C. A. van Helvoirt, M. A. Verheijen, W. M. Kessels, Atomic layer deposition of b-doped zno using triisopropyl borate as the boron precursor and comparison with al-doped zno, Journal of Materials Chemistry C 3 (13) (2015) 3095–3107.

[46] G. Haacke, New figure of merit for transparent conductors, Journal of Applied Physics 47 (9) (1976) 4086–4089.

[47] J. Manifacier, J. Gasiot, J. Fillard, A simple method for the determination of the optical constants n, k and the thickness of a weakly absorbing thin film, Journal of Physics E: Scientific Instruments 9 (11) (1976) 1002.

[48] R. Swanepoel, Determination of the thickness and optical constants of amorphous silicon, Journal of Physics E: Scientific Instruments 16 (12) (1983) 1214.

[49] T. Wei, P. Lan, Y. Yang, X. Zhang, R. Tan, Y. Li, W. Song, Tailoring the refractive index of aluminum doped zinc oxide thin films by co-doping with titanium, Applied Surface Science 263 (2012) 210–214.

[50] I. Horcas, R. Fernández, J. Gomez-Rodriguez, J. Colchero, J. Gómez-Herrero, A. Baro, Wsxm: a software for scanning probe microscopy and a tool for nanotechnology, Review of Scientific Instruments 78 (1) (2007) 013705.